Environ Monit Assess (2023) 195:58
https://doi.org/10.1007/s10661-022-10582-y

Classification of glacier with supervised approaches using PolSAR data

Ruby Panwar · Gulab Singh

Received: 7 February 2022 / Accepted: 11 July 2022 / Published online: 3 November 2022

Abstract Glacier comprises distinct features (snow, ice, and debris cover) and their identification and classification using satellite imagery is still a challenging task. Classification of different glacier features (zones) using remote sensing data is useful for numerous environmental and societal applications. The purpose of this study is to develop the fully polarimetric SAR (PolSAR) deep neural networks classification approach for the extraction of different features of the alpine glaciers. The developed approach was tested and classification results were compared with the support vector machines-based classification over the part of two glaciers: Siachen glacier and Bara Shigri glacier. The overall accuracy (OA) of GF-DNN classification is relatively high (91.17% for Siachen and 89% for Bara Shigri) with a good kappa coefficient (0.88 for Siachen and 0.85 for Bara Shigri) as compared to SVM for both the selected glaciers. An improvement of more than 10% is achieved in the OA of GF-DNN classification as compared to SVM for both the glaciers. The obtained classified results and accuracy demonstrates the potential of deep neural networks-based glacier features classification approach for glaciated terrain features.

R. Panwar (✉) · G. Singh
Centre of Studies in Resources Engineering, Indian Institute of Technology, Bombay, India
e-mail: rubypanwar17@gmail.com

G. Singh
e-mail: gulab.singh@iitb.ac.in

Keywords Glacier and its features · Radar remote sensing · GF-DNN · Support vector machines · Accuracy assessment

Introduction

Glaciers are the essential parts of the earth's cryosphere system. Glaciers are well known as an indicator of climatic variations, as climate fluctuations occur, the glacier also gets affected. In both hemispheres, mountain glaciers and snow cover have deteriorated on average and this worldwide retreat of glaciers and icecaps is making a substantial contribution to sea-level rise (Solomon et al., 2007). Many small glaciers that survived a few decades ago have now disappeared, and many existing glaciers today are more likely to go within a few more years (Zemp et al., 2006). It is the need of the hour to study glaciers and their facies distribution as well. Accumulation and ablation are two major facies/zones of the glacier (Williams et al., 1991). These two prime zones are the concatenation of various small zones formed on the glacier surface by snow accumulation, melting, and freezing, distribution of snow. It is very difficult to carry out field observations at each zone of the glacier, due to heavy glaciated rugged terrain. On the contrary, glacier features and zones can be classified using several machine learning algorithms (supervised or unsupervised) using satellite data (Kaushik et al., 2019). Discrimination of different

glacier features is directly or indirectly interlinked with other studies and can be used as a foundation that can be both global and environmental. Glacier facies and features are located at the different parts of the glacier.

Radar backscattering characteristics allow glacier classification (Singh et al., 2011, 2012, 2014; Singh & Venkataraman 2012). Different snow facies have distinct features, like backscattering signatures, density, grain size, and metamorphism (transformation of snow into ice) of snow influence these features (Benson, 1960; Cogley et al., 2011). The accurate mapping of different zones enables the accuracy of understanding climatic variability, weather forecasting, avalanche predictions, hydrological modeling, and mass-balance studies (Shukla & Ali, 2016). The rise in availability and accessibility of remote sensing data especially SAR images has shown the way to develop and employ newly automated and semi-automated techniques for glacier facies/zones classification. In past studies, researchers have used several algorithms for glacier facies identification using optical, infra-red, and radar images. But very limited studies related to glacier facies in the Himalayan Region using SAR datasets have been carried out (Huang et al., 2011; Sood, 2015; Kundu et al., 2015; Das et al., 2018, Pandey et al., 2020). Remotely sensed SAR images are more and more popular to be used for determining the glacier facies in the last decade. Considering the radar imagery over optical data has several advantages like penetration capability, good illumination conditions, and all-weather independence (Lee & Pottier, 2009; Rott & Matzler, 1987; Woodhouse, 2006).

Satellite datasets have been broadly used in the last few decades to delineate glacier features using automated or semi-automated classification methods and band ratios that report very high accuracy (Kaushik et al., 2019). Conventional statistical methods to more dominant machine learning algorithms provide superior versions of solutions to problem in the field of remote sensing for glaciated terrain classification. But the latest achievement of artificial intelligence brings new opportunities to the cryosphere field that is deep neural networks. Pandey et al. (2020) examined the effectiveness of maximum likelihood classifier over other classification methods adopted by many using multi-temporal SAR data for glacier facies mapping over the surge-type glacier in the Karakoram Range (Ahmad, 2012; Murtaza & Rhomsoo, 2014). Nijhawan et al. (2018) reveal the development of a hybrid deep learning framework by utilizing multi-phase deep learning and random forest by the ensemble of convolutional neural networks for delineation of supra-glacial debris lies in the parts of the Alaknanda basin in Uttarakhand. The Samudra Tapu glacier features were identified by utilizing integrated datasets from co-registered optical and thermal datasets into eight different classes using the maximum likelihood classifier, optical data helped in identifying supra-glacial cover types such as supra-glacial debris, ice, snow, mixed ice, and debris whereas thermal datasets used for differentiating non-supraglacial cover classes, like periglacial debris, valley rock, water, and shadow (Shukla et al., 2010). Kundu and Chakraborty (2015) examine Radarsat-2 polarimetric SAR data and time-series data of RISAT-1 MRS and hybrid data having RH/RV mode for the discrimination of different glacier radar facies of Gangotri and Samudra Tapu glacier. The major glacierized terrain features identified in these glaciers were wet or damp snow, debris-covered glacier ice, ice wall percolation area, ice walls, percolation area, and clean glacier ice.

The study reported in (Shukla & Yousuf, 2016) expresses the mapping of debris cover glaciers in Kashmir Himalaya using ASTER data and digital elevation model by the hierarchical knowledge-based classification method. The proposed HKBC approach used optical data having several input layers (such as NDSI, NDWI, and slope) and the overall accuracy of the study was found to be 89%. Bishop et al. (2008) marked the potential of artificial neural networks over the ISODATA clustering algorithm by estimating the different classes of supra-glacial debris loads of some Himalayan glaciers. They inspected the ANN approach for distinguishing spatial reflectance features in high-resolution SPOT panchromatic satellite imagery. In another study, Ban and Wu (2005) also examined in their comparative study for the classification of land use land cover features using ANN and MLC utilizing multi-temporal Radarsat images of the Greater Toronto Area, Canada. The authors claimed that ANN is more robust than MLC as observed in experimentation that the ANN approach provides improved classification accuracies of 4–6% compared to MLC. Shukla and Yousuf (2016) claim that the ANN-based information extraction method (OA-83.74%) performed superior to the maximum likelihood classifier (66.90%) for the mapping of

the Kalhoi glacier using Landsat TM data and other ancillary layers. The feasibility of polarimetric SAR satellite imagery in the field of glaciology for glacier zones and features classification has been improved by the rise of machine learning algorithms. Deep learning is one of the most adaptable up-to-date techniques for classification and a component of the broader family of machine learning techniques based on artificial neural networks.

In addition to the typical machine learning algorithms that have been used for glacier features mapping, an attempt have been made thru deep learning; an evolved practice of machine learning primarily founded upon neural networks and architectures with more hidden layers. Deep learning is a rapidly developing area within the fields of remote sensing and geo-informatics (Li et al., 2018; Ma et al., 2019; Zhang et al., 2016). Deep learning, as well as other artificial intelligence-based approaches, attempt to interpret images in the similar manner as a human machinist would, relying not only on pixel values but frequently occurring patterns and textures (Ma et al., 2019). As such, deep learning can be used to extract info from complex conditions where normal classification methods are not satisfactory (Li et al., 2018). Deep Learning algorithms consist of such a diverse set of models in comparison to a single traditional machine learning algorithm. This is because of the flexibility and feasibility that the neural network provides. To the best of our knowledge, there is a literature gap related to combining both "deep learning" and "radar glacier facies mapping" thematic. This study evolves in the direction of deep learning applications for glacier features classification, particularly related to fully polarimetric SAR images. Therefore, this study aims to develop a PolSAR classification algorithm by adopting the deep neural networks and support vector machines in glaciology for glacier facies/features identification. The utility of deep neural networks for multi-class classification using polarimetric SAR imagery has not yet been explored for glacier facies/features mapping. In this study, the deep neural networks-based PolSAR classification was carried out for identifying different glacier facies lying over the terrain. The SVM is selected to compare the results of (glacier facies–deep neural networks) GF-DNN approach because it is one of the robust, efficient, and most commonly used method for glaciology applications and it performs well with smaller training dataset also. The proposed glacier classification algorithm was implemented on the part of Siachen and Bara Shigri glaciers for assessing the performance and results were compared with the outcome of the support vector machines-based algorithm.

Glacier facies and their microwave response

Glacier surface features exhibit a range of zones—dry and wet snow, percolation, superimposed, bare ice, debris cover, etc. To better understand the varying conditions of a glacier's surface, the glacier surface area can be divided into a sequence of systematic, idealized zones, each of which is demarcated by a set of properties linking to the metamorphism of the snow or ice; zones range from dry snow at higher elevations to melting ice near the glacier snout/terminus (Williams et al., 1991). But not all glaciers will exhibit all zones. Though there are a wide collection of glacier facies, they can be pooled such that the glacier is divided into two larger areas: the accumulation zone and the ablation zone. In the percolation zone, the meltwater percolates a certain distance into the snowpack and refreezes to form inclusions of ice in the form of ice layers, ice-lenses, and pipe-like structures called ice glands. At microwave frequencies, the return of radar signals from ice lenses and ice pipes can be extremely high. However, the radar return is dependent on the topography, snow grain size, and dielectric properties of the terrain. In the ablation area, exposed/bare ice is followed by debris cover zone and dry snow zone generally has not been found in Himalayan glaciers. The different facies identified in the selected study area are given in Table 1 as follows:

The backscatter signal received back by the RADAR antenna is the sum of the surface scattering at the air/snow interface and the volume scattering within a snowpack. In the case of dry snow, the volume scattering is the dominant phenomenon that escalates with snow grain size and snow age. As the snow wetness increases the penetration capability of the SAR signal decreases and the volume scattering changes to surface scattering as a dominant scattering. The radar signal can penetrate more in the dry snow than the wet snow. There is a contrast in the backscatter signals between debris cover, bare ice, wet snow, and percolation that makes it possible to distinguish

Table 1 Glacier facies identified in the selected study area

Features/zones	Explanation
Percolation	Some surface melting occurs during the summer in this zone. The melt water percolates a certain distance into snow and refreezes to form inclusions of ice in the form of ice layers, lenses, and pipe-like structures called ice glands
Wet Snow	This zone generally lies at lower elevations and abundant surface melting occurs. Further down the percolation zone entire accumulation of current year's snow has melted
Bare ice	Bare ice facies is characterized by exposed ice surface throughout the year, subjected to constant melting. Snow that falls in this region quickly melts due to warmer temperatures, again exposing the existing ice
Debris cover	This type of glacier feature is generally found in young mountain ranges which are still elevating like Himalayan because of large rate of erosion that supply huge amount of debris in the form of gravel, rock, sand, and boulders onto the surface through landslides, avalanches, and rock falls. This region is separately classified as debris covered ice facies and extends until the snout/terminus of the glacier

different features. The altitudinal difference and the backscatter characteristics form the source of the detection of various features formed on the glaciated surface. In general, the accumulation zone is comprised of percolation zones and wet snow zones in the case of the Himalayan glaciers where in general

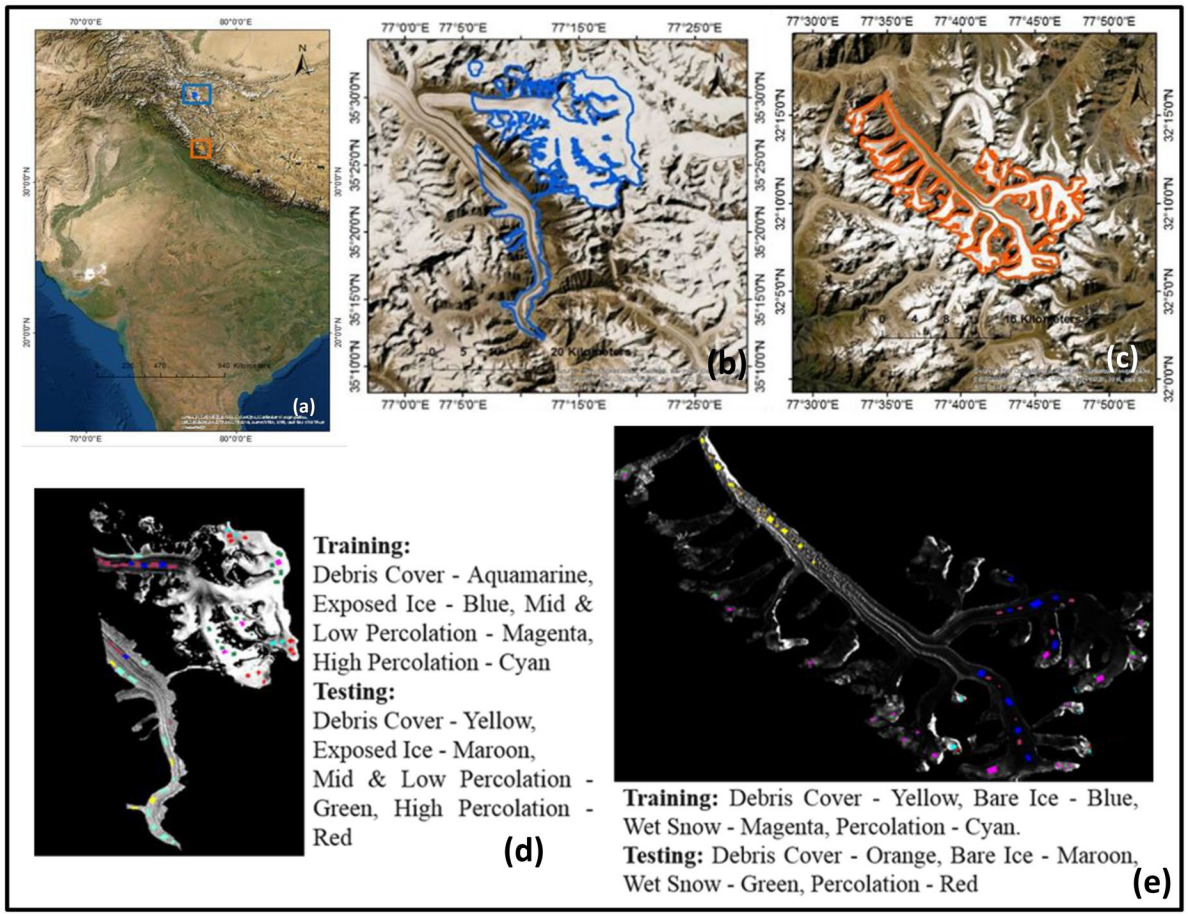

Fig. 1 Illustration of the study site. **a** Outline of India imagery with geographic location. **b** Map of sub-region of Siachen glacier. **c** Map of Bara Shigri glacier. **d**, **e** Training and testing samples selection over the PolSAR images

the dry snow zone is absent. The ablation zone of the Himalayan glaciers consists of bare ice and debris cover. The efficacy of glaciated terrain classification has associations for many related studies within glaciology. Variations in the extent of different zones are strictly associated with mass balance and, thus, they are of extreme concern to understand dynamics of the glacier and their association to climatic variations.

Study area and dataset used

Siachen glacier

It is located in the Karakoram Range of the North-Western Himalayas. It is the longest glacier in the Karakoram and the second-longest valley glacier in the world, outside the Polar Regions, extending in the northwest-southeast direction and spanning for a length of ~ 76 km. The terminus of the glacier is located at 3670 m.a.s.l., while the highest point in the accumulation zone is located at ~ 7200 m.a.s.l. The meltwater from this glacier feeds the Shyok River (a part of the Indus River system). The location and outline of the glacier are illustrated in Fig. 1a, b, respectively.

Bara Shigri

The Bara Shigri glacier is a few hundred kilometers south of Siachen Glacier. This glacier is located in the Chandra River Basin of Lahaul-Spiti Valley. It is heavily debris-covered, with much of it's in the ablation zone. The elevation ranges from 6250 m.a.s.l. at the highest point in the accumulation zone to 3975 m.a.s.l. at the snout, traversing the distance of 27.2 km between them. The Chandra River, which is one of the tributaries of the Indus River, receives meltwater from the Bara Shigri glacier. The location of the glacier and its outline are signified in Fig. 1a, c, respectively.

Datasets used

The Advanced Land Observing Satellite Using Phased-array L-band Synthetic Aperture Radar (ALOS PALSAR-1 and 2) is an earth observation satellite launched by JAXA (Japan Aerospace Exploration Agency). Both are active microwave remote sensing sensors having the capability to capture data day and night and in all weather conditions. The datasets detail utilized in this study is given in Table 2.

Methodology

PolSAR data and its processing

In this paper, fully polarimetric ALOS datasets used to classify the different glacier zones and multi-class glacier features lie in the study area. The SAR data were processed using the SNAP software packages. When an electromagnetic wave interacts with the target surface, it experiences some response and is reradiated back to the sensor; these responses are measured in the form of 2 × 2 scattering matrix [*S*] which is given by

$$[S] = \begin{bmatrix} S_{hh} & S_{hv} \\ S_{vh} & S_{vv} \end{bmatrix} \quad (1)$$

where each matrix element denotes the backscatter response of the target surface in a particular polarization. The complex backscatter response received in various polarimetric combinations is associated with the electrical and geometrical properties of the target surface. This 2 × 2 complex scattering matrix is not suitable to study natural targets, like snow and glaciers because they demonstrate a variety of scattering

Table 2 Technical details of acquired datasets

Satellite	ALOSPALSAR-1	ALOSPALSAR-2
Launch date	24 January 2006	24 May 2014
Date of acquisition	02 March 2009	08 April 2016
Level of data product	SLC, level 1.1	SLC, level 1.1
Polarization	Quad (HH, HV, VV, and VH)	Quad (HH, HV, VV, and VH)
Wavelength	L-Band	L-Band
Off-Nadir angle	21.5^0	33.2°
Location	N35°31′18.08″ and E76°57′3.77″	N32°9′38.48″ and E77°41′31.95″

responses. In such cases, the information obtained from the scattering matrix is inadequate to describe the physical properties of the target. Therefore, the second-order statistics of the scattering matrix—coherency matrix, utilized for this purpose. This coherency matrix [T] obtained from the scattering matrix by using its vectorized form derived from Pauli vector and can be given by (Lee & Pottier, 2009):

$$\langle [T] \rangle = \langle k_p k_p^T \rangle \tag{2}$$

where $\langle\rangle$ represents averaging over the whole data, k_p is Pauli vector given by

$$k_p = \frac{1}{\sqrt{2}} \begin{bmatrix} S_{hh} + S_{vv} \\ S_{hh} - S_{vv} \\ 2S_{hv} \end{bmatrix} \tag{3}$$

The coherency matrix [T] obtained from the above is

$$\langle [T] \rangle = \begin{bmatrix} \langle |S_{hh} + S_{vv}|^2 \rangle & \langle (S_{hh} + S_{vv})(S_{hh} - S_{vv})^* \rangle & 2\langle (S_{hh} + S_{vv}) S_{hv}^* \rangle \\ \langle (S_{hh} - S_{vv})(S_{hh} + S_{vv})^* \rangle & \langle |S_{hh} - S_{vv}|^2 \rangle & 2\langle (S_{hh} - S_{vv}) S_{hv}^* \rangle \\ 2\langle S_{hv}(S_{hh} + S_{vv})^* \rangle & 2\langle S_{hv}(S_{hh} - S_{vv})^* \rangle & 4\langle |S_{hv}|^2 \rangle \end{bmatrix} \tag{4}$$

Since the SAR images have a salt and pepper appearance called speckle noise, the presence of speckle noise may reduce the classification accuracy. So, to suppress the speckle noise it is necessary to perform multi-look in range direction as well as in azimuth direction. Using the digital elevation model (DEM), the terrain correction was applied to remove the geometric distortions. Further, the classification approaches have been implemented. The detailed architecture of the methodology followed in the work is displayed in Fig. 2.

Proposed classification approach

Two supervised classification approaches SVM and GF-DNN have been used. The number of classes that will classify considered was four using the PolSAR data for the study sites. Since the approaches used are supervised this requires a certain amount of learning data, so it is needed to create a training dataset. Different training sample/area was defined on the image for the different classes and each training area consists of multiple individual regions. The training samples over the study site were selected using ENVI software. The dataset has been divided into training data and testing data. The model learns on training data and is assessed on testing data. The details of both approaches have been discussed in further sections.

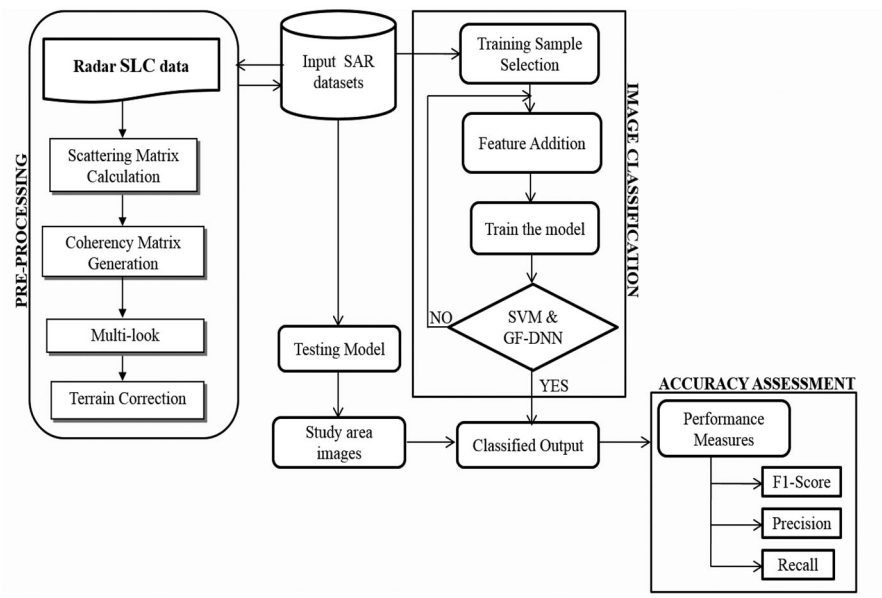

Fig. 2 Pictorial representation for methodology

Support vector machines

The support vector machines (SVM) is a commonly used supervised machine learning technique in remote sensing applications. Based on the data points/training samples, it creates a hyperplane that serves as a decision boundary. All training points are not used to construct the hyperplane but it only includes the point that lies nearer to the hyperplane and these points are called support vectors. A linear support vector machine may not be able to separate the classes in some circumstances; in these cases, we must map the classes onto a higher-dimensional space to improve class separation. Various kernel functions are employed to map the training samples into higher-dimensional space, allowing for easier fitting of a linear hyperplane (Tso & Mather, 1995; Cortes & Vapnik, 1995). SVM kernel selected is the radial basis function (RBF) utilized to map the classes in a higher-dimensional space to obtain an optimal separation plane in such non-linear classification cases. This function can be mathematically characterized as follows:

$$K(X_1, X_2) = exp\left(-\frac{\|X_1 - X_2\|^2}{2\sigma^2}\right) \quad (5)$$

where σ is the variance and $\|X_1 - X_2\|$ is the Euclidean distance between two points.

For multiclass classification, ENVI's version of SVM employs the pair-wise classification technique. The decision values of each pixel for each class are used for probability estimations in the SVM classification output. ENVI classifies data by choosing the option with the highest probability. Pixels with all probability values less than the threshold can be reported as unclassified using an optional threshold. SVM provides a penalty option that allows for some misclassification, which is especially crucial when working with non-separable training sets. The penalty parameter regulates the trade-off between allowing for training errors and enforcing strict margins (SVM Tutorial, 2020). Repeated attempts with varying *C* (cost or penalty parameter) and gamma, γ (trial and error method) helps in defining these parameters based on the accuracy of the classified output. An ENVI software used to test the multiple values of variables *C* and γ, to fine tune the parameters and find optimal values to be used for classification. The definition of the parameters used for SVM approach are provided in Table 3 as follows:

Table 3 Definition of the parameters used for SVM

Support vector machine RBF	Parameter value
Gamma in kernel function	*0.01*
Penalty parameter	*100.00*
Pyramid levels	*1.00*
Pyramid reclassification threshold	*0.90*
Classification probability threshold	*0.00*

Deep neural networks

A multi-layered deep neural network (DNN) with error back-propagation is the sort of deep learning architecture used in this study. DNN is a type of neural network that connects various functions in a hierarchically structured network with hidden layers. Nowadays, the classification of features has also profited from the applications of SAR deep learning approaches. There has been a lot of research going on to explore the feasibility of deep learning for several applications such as identifying oil spills, the thickness of sea ice, sea ice classification, and many more. The basic architecture of deep neural networks for glaciated terrain features classification is shown in Fig. 3.

The number of nodes in the input layer corresponds to the number of input variables chosen. A dense layer called the fully connected layer was used in this study to develop the GF-DNN model. The information travels from the input data to the activation function, the error is calculated and propagated back to the previous levels, and the output is fed at the end of the predefined iteration (Goodfellow et al. 2016). In this approach, until the output layer, each sequential hidden layer mixes values from the previous layer and then learns to build more abstract representations. For each hidden layer in the model, the rectified linear unit activation function has been chosen and softmax activation in the output layer. And to finish it off, the model was compiled with Adam optimizer and using cross-entropy for the loss function. The dense layer in deep learning can be defined as, $a = activation(w * x + b)$ where '*w*' is weight, '*x*' is input, '*b*' is bias, 'a' is output, and '*' matrix

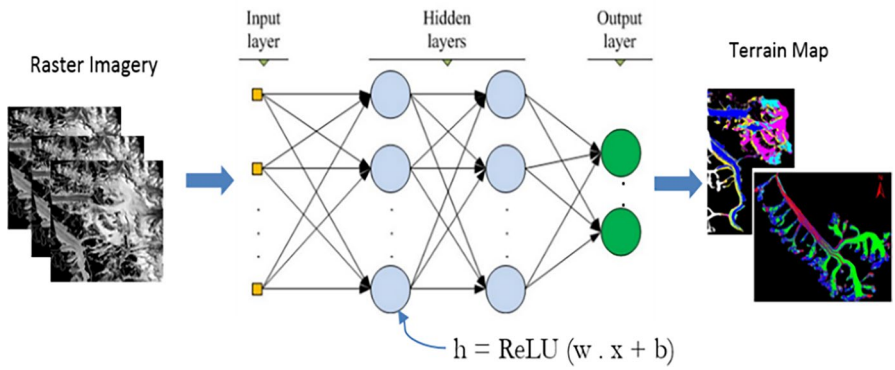

Fig. 3 Deep neural networks in cryosphere

multiplication. The definition of the parameters used for GF-DNN approach are provided in Table 4 as follows:

Keras tuner used for getting the best parameters for the proposed model, i.e., GF-DNN for the highest accuracy. Keras tuning is a package that helps users identify the best hyper-parameters for machine learning and deep learning models. Kernel sizes, learning rates for optimization, and various hyper-parameters may all be found with the package. A python program, which iterates multiple times with different parameter values, to fine tune the parameters was used to find optimal values to be used for classification. A non-linear activation function needs to be introduced at each network layer since the relationship between input and output should be a highly non-linear mapping. Due to saturating non-linearity of other activation functions, ReLU has been involved in this study. The ReLU activation function is given by

$$f(x) = \max(0, a) where\ a = (w^{*}x + b) \tag{6}$$

The non-linear activation function allows the back-propagation and also allows to stack number of layers of neurons to create a DNN. Moreover, deep neural networks using ReLU achieved the best performance and considerably takes less training time. The softmax non-linearity is applied to the output layer for multi-class classification. This function will output the posterior probabilities for each possible class. Mathematically, the softmax formula is as follows:

$$\text{softmax}, \sigma(\vec{z})_i = \frac{e^{z_i}}{\sum_{j=1}^{K} e^{z_j}} \tag{7}$$

where e^{z_i} is the exponential function applied to each element of the input vector and the $\sum_{j=1}^{K} e^{z_j}$ is the normalization form that confirms all the output values of the function sum to one, thus creating the valid probability distribution and, K represents a number of classes in the multi-class classifier. Cross entropy is the loss function for this multi-class classification problem and can be calculated by

$$P = -\sum Y_i^{'}.\log\left(Y^i\right) \tag{8}$$

where $Y_i^{'}$ are actual probabilities and Y^i are computed probabilities. Drop-out is an extremely effective and efficient regularization technique to reduce overfitting. The backpropagation is used to train the network and it computes the error term for every unit in the network. The training of BPN will have the following phases as shown in Fig. 4:

The output signal of the network 'y' is compared with the desired output value and the difference is called error signal d of the output layer neuron computed as

$$Loss\ function, \partial = z - y \tag{9}$$

It is commonly useful to reduce the learning rate during training. In this paper, initially, the learning

Table 4 Definition of the parameters used for DNN

Hyper-parameter	Value/definition
Learning rate	*0.01*
Drop-out	*0.1*
Activation	*ReLu*
Optimizer	*Adam*
No. of epochs	*2000*
Classifier	*Softmax*

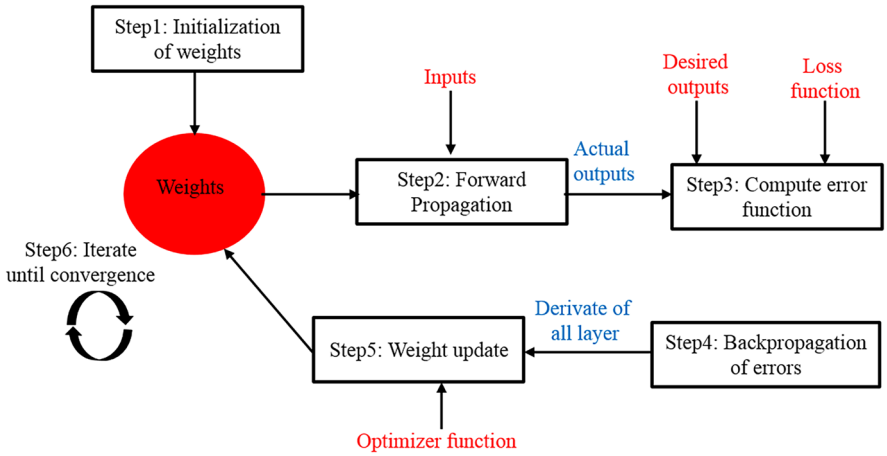

Fig. 4 Backpropagation—learning

rate is 0.001 but after certain epochs, it is reduced to 0.01 where epochs represent the number of times each sample has been used in training. As the network gets trained, then it is ready to make predictions on the test data and then the performance metrics of the model have been evaluated which gives the visualization of the performance of the approach.

Accuracy assessment of the classification results

The accuracy of the classifier is assessed to assure its credibility. Among the various available metrics, precision, recall, F1score, overall accuracy, and kappa coefficient is used for assessing classifiers. Overall, accuracy is the most widely used metric which helps in easy interpretation and is effective in accuracy estimation. It expresses the percentage of test data which has been correctly classified by the classifier. The relationship between true positives and the overall number of true positives and false positives is referred to as precision. The number of true positives to the total number of true positives and false negatives is known as recall. The F1 score is the harmonic mean of the precision and recall, and it seeks to characterize their balance. Following are the formulas used to evaluate the performance measures:

$$Precision = (Total\ positive)/(Total\ positive + False\ positive)$$

$$Recall = (Total\ positive)/(Total\ positive + False\ negative)$$

$$F1\ Score = (2 * precision * recall)/(precision + recall)$$

Additionally, with an intention to further evaluate the class-level performance of a given classifier, confusion matrices are generated for used approaches. Another aspect of focus is to understand the performance of GF-DNN and SVM models when compared to each other. The relative comparison is performed using *Z*-score as described in Rossiter (2014). To evaluate the significance of the output of two classifiers, the z-score calculated by the formula:

$$z = \frac{|p_1 - p_2|}{\sqrt{s_1^2 + s_2^2}}$$

where p1 and p2 denote the proportions of the correctly classified test data of the two classifiers while s1 and s2 represent the standard deviation of their samples. Field collected points reflecting distinct radar facies on the glacier surface should ideally be used to assess classification quality. The accuracy of the classification can be estimated by comparing the information class collected in the field with that derived from the classed output image. Due to the lack of field data for this investigation, a test set is constructed in parallel using a technique similar to that used to generate a training set in ENVI.

Results and discussions

For the mountain cryosphere, machine learning and deep learning models can be applied to classification, feature identification, automatic mapping, and visual

interpretation tasks as well as time series simulations. Deep learning methods for cryosphere applications are still scarce. Only 2% of studies using deep learning-based image segmentation and object detection have looked into cryosphere-related issues (Hoeser & Kuenzer, 2020). Machine learning applications on alpine or mountain glaciers emphasis on determining the glacier extent by either extracting the calving front (Baumhoer et al., 2019; Cheng et al., 2020) or detecting the glacier boundary of debris covered glaciers (Khan et al., 2020; Nijhawan et al., 2018; Xie et al., 2020). The potential of deep learning in glaciology in terms of automation, efficient processing, and the reduction of traditionally laborious manual tasks, is slowly being realized, although it still has untapped potential. This study reveals the unexploited potential of deep learning-based glacier facies mapping on the mountain cryosphere using quad-polarimetric SAR datasets.

The support vector machines and deep neural networks-based methods have been applied on fully polarimetric SAR data over the sub-part of Siachen and Bara Shigri glacier for the identification of distinct glacier facies/zones. In general, the radar glacier zones follow the elevational zonation like dry snow, percolation zone, wet snow zone, bare ice zone are distributed successively from higher to lower elevations of glaciers (Partington, 1998). The elevation map is given in Figs. 5b and 6b gives the idea about the appropriate altitudinal pattern for different glaciated features lying over the terrain. The results from radar data analysis show a general trend of facies distribution on the surface of the glacier. In the case of the Siachen sub-part, the facies follow an altitudinal pattern with a high percolation zone followed by mid and low percolation zone located at the higher reaches (dry snow in case it is present) and exposed ice followed by debris cover at the lowest reaches of the glacier. For the Bara Shigri glacier, the pattern is like a percolation zone followed by a wet snow zone located at the higher reaches (dry snow absent) and bare ice followed by debris cover at the lower elevation of the glacier. The slope values are also very high for the accumulation area because of the steep slope and low for the ablation zone for both the glaciers. In the classified output image for Siachen sub-part Fig. 5c, d, four different zones of the glacier (high percolation, mid and low percolation, exposed ice, debris cover) were identified following the elevation pattern.

Generally, upper percolation facies was only found over sub-part of Siachen glacier due to the intense freezing conditions that the glacier is exposed to throughout the year. The Bara Shigri glacier is at a lower elevation, it is subjected to milder weather conditions that are not conducive to the presence of upper percolation facies. In the above Fig. 5c, d, both the approaches provide very good assessments of different features, but SVM gives typical misclassification of numerous pixels. The area inside the green and red circle in Fig. 5c shows the several pixels wrongly classified as percolation pixels of debris cover are displayed whereas by DNN these pixels are correctly classified in Fig. 5d.

For Bara Shigri glacier, due to the early summer melting of compact dry snow, the upper percolation zone does not exist in this location. So, the middle percolation zone is the sole percolation facie K is found in the Bara Shigri Glacier. As the seasons change from winter to summer, the temperature rises significantly, causing substantial melting and the disappearance of the lower percolation zone. The accumulation zone that consists of percolation and wet snow facies for Bara Shigri glacier. The ablation zone of the glacier, consisting of debris cover and bare ice. From the classified maps, presented in Fig. 6d, it can be seen debris cover is extensive in case of Bara Shigri glacier. In Bara Shigri output Fig. 6c, the percolation and wet snow pixels inside the yellow box are misclassified as bare ice pixels and grey box are debris cover pixels misclassified as wet snow whereas in Fig. 6d it is improved and shows the correctly identified percolation and wet snow pixels (in yellow box Fig. 6d) and debris cover pixels (in grey box Fig. 6d). It is seen that using SVM, there is a lot of misclassification between the classified pixels but up to a certain extent this is overcome by the DNN approach. To ensure that the results are not biased by using the same ROIs used for classification, new ROIs are employed to compute the confusion matrix. The confusion matrix provides an independent accuracy review of the classification map in this way. In this study, an accuracy assessment has been carried out to test the accuracy level of classified maps generated by SVM and GF-DNN for the datasets used. We found that the overall accuracy of DNN is more as compared to SVM for both the glacier and below are the confusion matrices provided in Tables 5 and 6.

Precision, recall, and F1-score performance measures have been used to evaluate the performance of

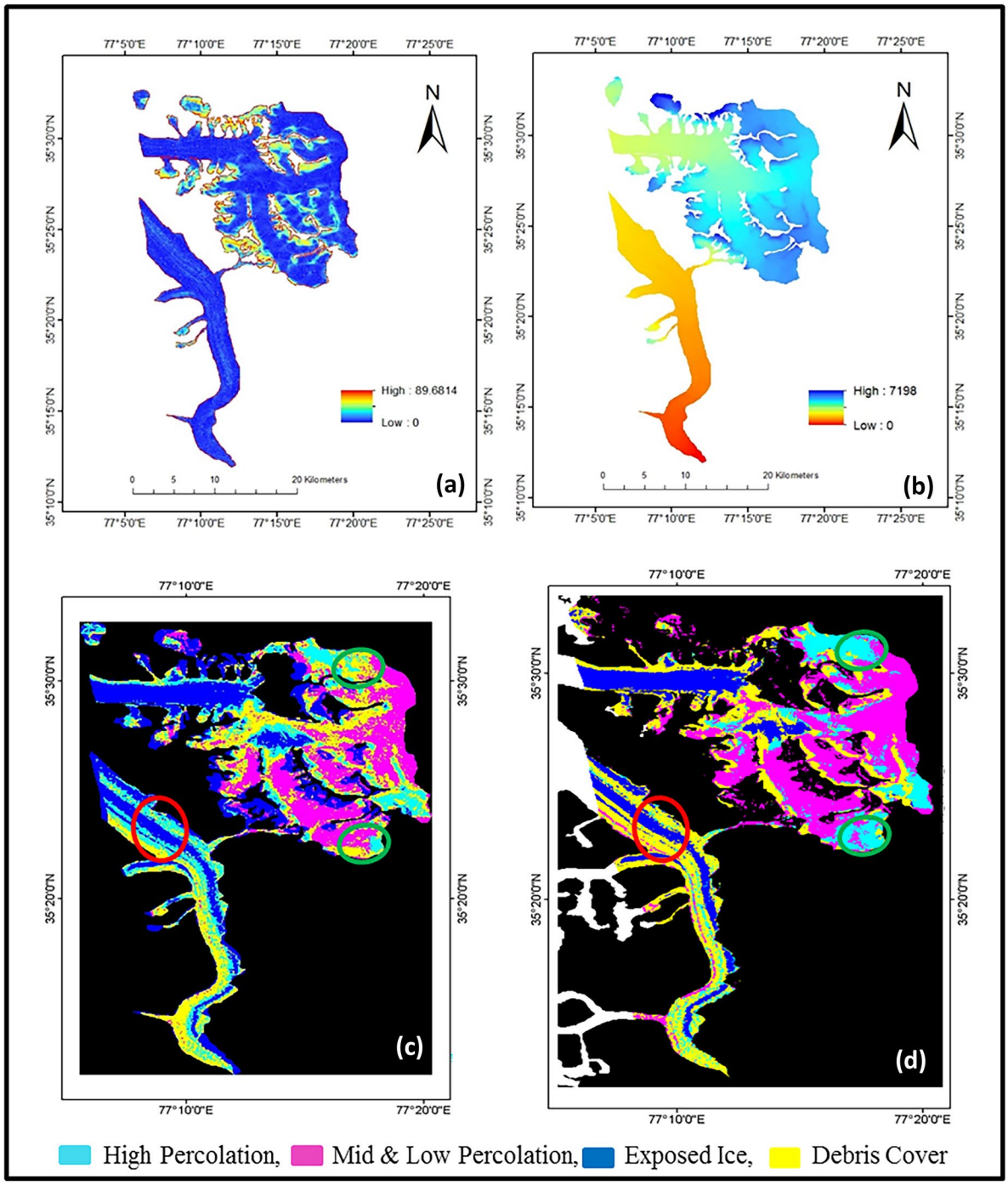

Fig. 5 Sub-part of Siachen glacier: **a** Slope map. **b** Elevation map. **c** Classified map using SVM, area inside the red and green circle shows the misclassification of debris cover class into percolation class and vice-versa. **d** Classified map using GF-DNN, red and green circles indicate correctly classified area

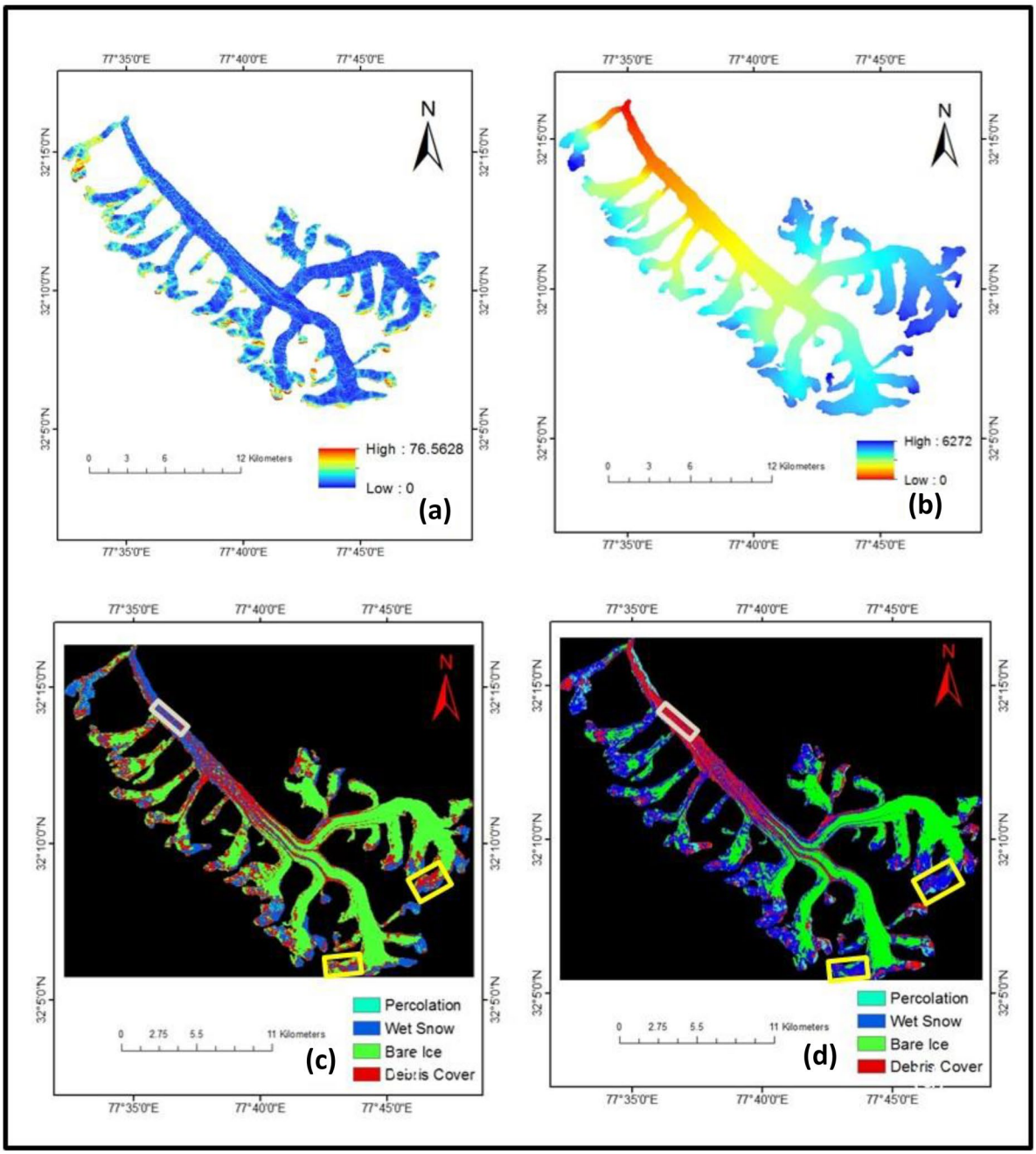

Fig. 6 Bara Shigri glacier. **a** Slope map. **b** Elevation map. **c** Classified map using SVM, pixels inside the yellow boxes shows wrongly classified as debris cover and bare ice at higher reaches. **d** Classified map using GF-DNN, yellow boxes indicates the correctly classified pixels as debris cover and bare ice at higher reaches

the model for the study area. The kappa coefficient was utilized as an accuracy metric in this investigation. The standard values for the kappa coefficient follow: value 0.8 or higher indicates good agreement, 0.4–0.8 indicates moderate agreement, and less than 0.4 indicates poor agreement. Table 7 includes the evaluation metrics for study area images.

Table 5 Siachen glacier sub-part—confusion matrices: (a) SVM (b) GF-DNN

(a)

SVM		Actual class				
(OA = 80.49%)		High percolation	Mid and low percolation	Exposed ice	Debris cover	Total
Predicted class	High percolation	**167**	0	3	208	378
	Mid and low percolation	52	**400**	0	12	464
	Exposed ice	0	0	**573**	1	574
	Debris cover	91	24	0	**473**	588
	Total	310	424	576	694	**2004**

(b)

DNN		Actual class				
(OA = 91.17%)		High percolation	Mid and low percolation	Exposed ice	Debris cover	Total
Predicted class	High percolation	**575**	0	0	1	576
	Mid and low percolation	2	**520**	108	64	694
	Exposed ice	0	0	**424**	0	424
	Debris cover	0	0	2	**308**	310
	Total	577	520	534	373	**2004**

A combination of high recall and high precision is required for a classifier to be rated highly accurate. Precision and recall are the terms used to describe the user and producer accuracy, respectively (Taubenbock et al., 2011). GF-DNN produced superior precision and recall scores which, as expected, generated a higher F1 score as well. It is to be observed that precision values obtained for different classes are well and good over the study area using DNN. The overall accuracy with GF-DNN is found to be 91.17% and the kappa coefficient

Table 6 Bara Shigri glacier—confusion matrices: (a) SVM (b) GF-DNN

(a)

SVM		Actual class				
(OA = 58.86%)		Percolation	Wet snow	Bare ice	Debris cover	Total
Predicted class	Percolation	**27**	23	0	31	81
	Wet snow	280	**627**	0	699	1606
	Bare ice	14	94	**1499**	20	1627
	Debris cover	37	566	2	**374**	979
	Total	358	1310	1501	1124	**4293**

(b)

DNN		Actual class				
(OA = 89%)		Percolation	Wet snow	Bare ice	Debris cover	Total
Predicted class	Percolation	**223**	39	0	82	344
	Wet snow	17	**1237**	20	95	1369
	Bare ice	0	11	**1490**	0	1501
	Debris cover	29	148	1	**901**	1079
	Total	269	1435	1511	1078	**4293**

Table 7 Performance metrics: (a) sub-part of Siachen glacier (b) Bara Shigri glacier

(a)						
Class	SVM			GF-DNN		
	Precision	Recall	F1-score	Precision	Recall	F1-score
High percolation	0.44	0.54	0.51	0.99	0.99	0.99
Mid and low percolation	0.86	0.94	0.89	0.75	1	0.86
Exposed ice	0.99	0.99	0.99	1	0.79	0.88
Debris cover	0.8	0.68	0.74	0.99	0.83	0.9
Total	0.77	0.79	0.78	0.93	0.9	0.91
(b)						
Class	SVM			GF-DNN		
	Precision	Recall	F1-score	Precision	Recall	F1-score
Percolation	0.33	0.07	0.12	0.65	0.83	0.73
Wet snow	0.39	0.47	0.43	0.9	0.86	0.88
Bare ice	0.78	0.99	0.87	0.99	0.98	0.98
Debris cover	0.38	0.33	0.35	0.83	0.83	0.83
Total	0.47	0.46	0.44	0.84	0.87	0.86

0.88 for sub-part of Siachen glacier whereas in the case of Bara Shigri glacier 89% and kappa coefficient 0.85 which shows a very good agreement between the predicted output and the actual output. Studies by Huang et al., 2013; Sood, 2015; Kundu & Charakborty, 2015; Pandey et al., 2020, show such results for maximum likelihood classifier, random forest, support vector machine and others but the implementation of deep neural networks using fully polarimetric radar data for glacier facies mapping has not been studied so far. In this study, we found that the deep neural network model shows very good convergence behavior for classification accuracy as compared to other machine learning approaches. By comparing the results from the SVM and the DNN, we demonstrates that the DNN yields more accuracy for selected study regions.

To affirm the significance of results and performance between classifiers considered in the study,

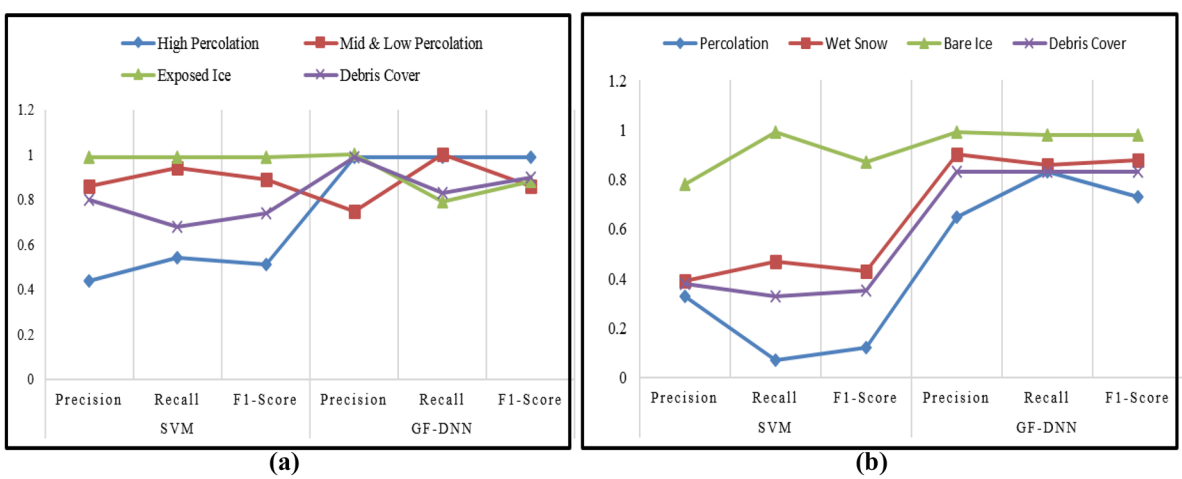

Fig. 7 Graphical illustration of performance metrics. **a** Siachen glacier sub-part. **b** Bara Shigri glacier for individual classes with SVM and DNN

Z-test is performed. *Z*-scores indicate the significantly higher performance of GF-DNN over the SVM classifier. GF-DNN performs better than SVM 86.8% for Bara Shigri and 95.9% for sub-part of Siachen glacier and the results of *Z*-test score between GF-DNN and SVM is 1.75 for Bara Shigri case while for Siachen sub-part the value is 1.12. Accuracies of glacier classified maps also depend on the classifiers. Upon comparison we observed that GF-DNN model performed relatively well for both datasets, while SVM showed a decrease in performance as shown in Fig. 7 below:

It is largely agreed that SAR images are one of the most appropriate tool in glacier radar facies/zones mapping (Akbari et al., 2013; Fu et al., 2020; Huang et al., 2013; Zhou & Zheng, 2017). Day-night acquisition and cloud free imageries make the SAR applications requisite for glacier studies. Over mountainous terrains, accuracies might be affected by geometric distortions caused by side-looking SAR acquisition geometry. The past and ongoing studies recommends increasing the implementation of SAR data in different glacier studies (radar zones, mass balance, dry or wet ice, surface dynamics, etc.) in the polar and non-polar regions. It can be concluded that geospatial techniques can make the glacier facies studies possible without field survey. However, outcomes from satellite imageries should be substantiated with field observed information.

Conclusion

In this study, we have presented a novel application of the GF-DNN model using quad-pol datasets for the identification of different glacier facies, with better accuracy of classified maps. Both the approaches GF-DNN and SVM were applied on two alpine glaciers (namely sub-part of Siachen glacier and Bara Shigri glacier) and produced a very promising output in both cases using GF-DNN. The major glacier radar facies identifiable and classified using such data and methods are high percolation, mid and low percolation, exposed ice, and debris-cover zone in sub-region of Siachen glacier and Bara Shigri facies are percolation, wet snow, bare ice and debris cover followed by altitudinal pattern. Such information can be used to find the glaciers accumulation and ablation area, which can further be used as input to glacier mass balance models and to understand the dynamics of a glacier.

The accuracy assessment of both methods shows that DNN maps were considered to have better accuracy than the SVM-based classified maps. Though the classification accuracies for every class with DNN are considerably fine still put up with some misclassification that needs further work to be done. However, the accuracy of the model could be enhanced much more with the parametrization of the network because it extremely depends on the structure of the neural network. Assessments over different areas of Himalayan Region ought to additionally be performed further.

Acknowledgements The authors are grateful to Japanese Space Exploration Agency (JAXA) for providing the desired fully polarimetric Quad-Pol ALOS-1 and ALOS-2 datasets to carry out this work. This work was supported by the Department of Science and Technology, Govt. of India under the project DST/CCP/NHC/155/2018(G).

Declarations

Conflict of interest The authors declare that they have no competing interests.

References

Ahmad, A. (2012). Analysis of maximum likelihood classification on multispectral data. *Applied Mathematical Sciences, 6*(129), 6425–6436.

Akbari, V., Doulgeris, A. P., & Eltoft, T. (2013). Monitoring glacier changes using multitemporal multipolarization SAR images. *IEEE Transactions on Geoscience and Remote Sensing, 52*, 3729–3741.

Ban, Y., & Wu, Q. (2005). RADARSAT DAR data for land-use/land-cover classification in the rural-urban fringe of the Greater Toronto Area. *Proceedings of 8th AGILE Conference on Geographic Information Science, Estoril, Portugal.*

Baumhoer, C. A., Dietz, A. J., Kneisel, C., et al. (2019). Automated extraction of Antarctic glacier and ice shelf fronts from Sentinel-1 imagery using deep learning. *Remote Sensing, 11*(21), 2529.

Benson, C. S. (1960). Stratigraphic studies in the snow and firn of the Greenland ice sheet. *Cold Regions research and engineering Lab, Hanover, Report, 70*.

Bishop, M. P., Shroder, J. F., & Hickman, B. L. (1999). SPOT panchromatic imagery and neural networks for information extraction in a complex mountain environment. *Geocarto International*. https://doi.org/10.1080/10106049908542100

Cheng, D., Mohajerani, Y., Wood, M., et al. (2020). Calving Front Machine (CALFIN): Automated calving front dataset and deep learning methodology for East/West Greenland, 1972–2019. Retrieved December 7, 2021, from https://meetingorganizer.copernicus.org/EGU2020/EGU2020-19979.hmtl

Cogley, J. G., Hock, R., Rasmussen, L. A., Arendt, A. A., Bauder, A., Braithwaite, R. J., Jansson, P., Kaser, G., Möller, M., Nicholson, L., & Zemp, M. (2011). Glossary of glacier mass balance and related terms. IHP-VII technical documents in hydrology No. 86, IACS Contribution no. 2.

Cortes, C., & Vapnik, V. (1995). Support-vector networks. *Machine Learning., 20*(3), 273–297.

Das, S., Sanid, C., Chakraborty M., & Misra A. (2018). Himalayan glacial facies detection and monitoring using SAR Data. *ISG NEWSLETTER*, vol. 24, no.3 & 4.

Fu, W., Li, X., Wang, M., & Liang, L. (2020). Delineation of Radar Glacier Zones in the Antarctic Peninsula Using Polarimetric SAR. *Water, 12*(9), 2620. https://doi.org/10.3390/w12092620

Goodfellow, I., Bengio, Y., & Courville, A. (2016). Chapter 6: deep feed-forward networks. In: Deep Learning. Massachusetts: MIT Press, pp. 168–224.

Hoeser, T., & Kuenzer, C. (2020). Object detection and image segmentation with deep learning on earth observation data: A review–Part I: Evolution and recent trends. *Remote Sensing, 12*(10), 1667.

Huang, L., Li, Z., Tian, B., Chen, Q., Liu, J., & Zhang, R. (2011). Classification and snow line detection for glacial areas using the polarimetric SAR image. *Remote Sensing of Environment*, *115*(7), 1721–1732.

Huang, L., Li, Z., & Tian, B. (2013). Monitoring glacier zones and snow/firn line changes in the Qinghai-Tibetan Plateau using C-band SAR imagery. *Remote Sensing of Environment, 137*, 17–30.

Kaushik, S., Joshi, P. K., & Singh, T. (2019). Development of glacier mapping in Indian Himalaya: A review of approaches. *International Journal of Remote Sensing, 40*(12), 1–28. https://doi.org/10.1080/01431161.2019.1582114

Khan, A. A., Jamil, A., Hussain, D., Taj, M., Jabeen, G., & Malik, M. K. (2020). Machine learning algorithms for mapping debris-covered glaciers: The Hunza Basin case study. *IEEE Access, 8*, 12725–12734.

Kundu, S., & Chakraborty, M. (2015). Delineation of glacial zones of Gangotri and other glaciers of Central Himalaya using Risat-1 C-band dual-pol SAR. *International Journal of Remote Sensing, 36*(6), 1529–1550. https://doi.org/10.1080/01431161.2015.1014972

Lee, J.S., & Pottier, E. (2009). *Polarimetric radar imaging: from basics to applications* (1st edition) CRC Press.

Li, Y., Zhang, H., Xue, X., Jiang, Y., & Shen, Q. (2018). Deep learning for remote sensing image classification: a survey. *Wiley Interdisciplinary Reviews: Data Mining and Knowledge Discovery*, *8*(6). https://doi.org/10.1002/widm.1264

Ma, L., Liu, Y., Zhang, X., Ye, Y., Yin, G., & Johnson, B. A. (2019). Deep learning in remote sensing applications: A meta-analysis and review. *ISPRS Journal of Photogrammetry and Remote Sensing, 152*, 166–177. https://doi.org/10.1016/j.isprsjprs.2019.04.015

Murtaza, K. O., & Romshoo, S. A. (2014). Determining the suitability and accuracy of various statistical algorithms for satellite data classification. *International Journal of Geomatics and Geosciences*, *4*(4).

Nijhawan, R., Das, J., & Raman, B. (2018). A Hybrid CNN + random forest approach to delineate debris covered glaciers using deep features. *Journal of the Indian Society of Remote Sensing, 46*, 981–989. https://doi.org/10.1007/s12524-018-0750-x

Pandey, P., Singh, R., Prasad, A. V., Mahagoankar, A. V., & Ali, S. N. (2020). Facies detection of surge-type glaciers, Karakoram Himalaya using Sentinel-1 Images. *Geocarto International, Taylor & Francis.* https://doi.org/10.1080/10106049.2020.1801856

Partington, K. (1998). Discrimination of glacier facies using multi-temporal SAR data. *Journal of Glaciology, 44*(146), 42–53. https://doi.org/10.3189/S0022143000002331

Rossiter, D. G. (2014). Statistical methods for accuracy assessment of classified thematic maps. Retrieved January 18, 2022, from www.itc.nl/personal/rossiter

Rott, H., & Matzler, C. (1987). Possibilities and limits of synthetic aperture radar for snow and glacier surveying. *Annals of Glaciology, 9*, 195–199. https://doi.org/10.3189/S0260305500000604

Shukla, A., & Ali, I. (2016). A hierarchical knowledge-based classification for glacier terrain: a case study from Kalhoi Glacier, Kashmir Himalaya. *Annals of Glaciology*, *57*, 71. https://doi.org/10.3189/2016AoG71A046

Shukla, A., Gupta, R. P., & Arora, M. K. (2010). Delineation of debris covered glacier boundaries using optical and thermal remote sensing data. *Remote Sensing of Letters, Taylor Ad Francis, 1*(1), 11–17. https://doi.org/10.1080/01431160903159316

Shukla, A., & Yousuf, B. (2016). Evaluation of multisource data for glacier terrain mapping: a neural net approach. *Geocarto International*, *32*(5). https://doi.org/10.1080/10106049.2016.1161078

Singh, G., Venkataraman, & Park, S. E. (2011). Utilization of four-component scattering power decomposition method for glaciated terrain classification using fully polarimetric PALSAR data. *Geocarto International*, *26*(5), 377–389. https://doi.org/10.1080/10106049.2011.584978

Singh, G., & Venkataraman, G. (2012). Application of incoherent target decomposition theorems to classify snow cover over the Himalayan region. *International Journal of Remote Sensing, 33*(13), 4161–4177. https://doi.org/10.1080/01431161.2011.639402

Singh, G., Venkataraman, G., Yamaguchi, Y., & Park, S. E. (2014). Capability assessment of fully polarimetric ALOS-PALSAR data for discriminating wet snow from othet scattering types in mountainous regions. *IEEE Transcations on Geoscience and Remote Sensing, 52*(2). https://doi.org/10.1109/TGRS.2013.2248369

Singh, G., Yamaguchi, Y., & Park, S. E. (2012). Evaluation of modified four-component scattering power decomposition method over highly rugged glaciated terrain. *Geocarto International, 27*(2), 139–151. https://doi.org/10.1080/10106049.2011.626082

Solomon, S., Qin, D., Manning, M., Chen, Z., Marquis, M., Averyt, K., Tignor, B., & Miller, H. (2007). *Fourth assessment report of the intergovernmental panel on climate change*. Cambridge University Press.

Sood, S. (2015). Glacier classification and movement estimation using SAR polarimetric and interferometric techniques, *IIRS-ITC joint Master of Science in Geoinformation Science and Earth Observation (MSc) thesis of the University of Twente.*

SVM Tutorials. (2020). Harris Geospatial Solutions, Inc. Retrieved November 11, 2021, from https://www.l3harrisgeospatial.com/docs/backgroundsvmgeneral.html

Taubenbock, H., Esch, T., Felbier, A., Roth, A., & Dech, S. (2011). Pattern-based accuracy assessment of an urban footprint classification using TerraSAR-x data. *IEEE Geoscience and Remote Sensing Letters, 8*(2), 278–282. https://doi.org/10.1109/LGRS.2010.2069083

Tso, B., & Mather, P. (1995). Classification methods for remotely sensed data. Second Edition, *Taylor & Francis.*

Williams, R. S., Hall, D. K., & Benson, C. S. (1991). Analysis of glacier facies using satellite techniques. *Journal of Glaciology, 37*(125), 120–128. https://doi.org/10.3189/S0022143000042878

Woodhouse, I. H. (2006). Introduction to microwave remote sensing, *CRC Press, Taylor & Francis Group.*

Xie, Z., Haritashya, U. K., Asari, V. K., et al. (2020). GlacierNet: A deep-learning approach for debris-covered glacier mapping. *IEEE Access, 8*, 83495–83510.

Zemp, M., Haeberli, W., Hoelzle, M., & Paul, F. (2006). Alpine glaciers to disappear within decades. *Geophysical Research Letters*, *33*(13). https://doi.org/10.1029/2006GL026319

Zhang, L., Zhang, L., & Du, B. (2016). Deep learning for remote sensing data: A technical tutorial on the state of the art. *IEEE Geoscience and Remote Sensing Magazine, 4*(2), 22–40. https://doi.org/10.1109/MGRS.2016.2540798

Zhou, C. X., & Zheng, L. (2017). Mapping radar glacier zones and dry snow line in the Antarctic Peninsula using Sentinel-1 images. *Remote Sens., 9*, 1171.